NANO LETTERS

Letter

Cite This: Nano Lett. XXXX, XXX, XXX−XXX

pubs.acs.org/NanoLett

Long Exciton Dephasing Time and Coherent Phonon Coupling in $CsPbBr_2Cl$ Perovskite Nanocrystals

Michael A. Becker,[†,‡] Lorenzo Scarpelli,[§] Georgian Nedelcu,[∥,⊥] Gabriele Rainò,[∥,⊥] Francesco Masia,[§] Paola Borri,[§,#] Thilo Stöferle,[†] Maksym V. Kovalenko,[*,∥,⊥] Wolfgang Langbein,[*,§] and Rainer F. Mahrt[*,†]

[†]IBM Research−Zurich, Säumerstrasse 4, 8803 Rüschlikon, Switzerland

[‡]Optical Materials Engineering Laboratory, ETH Zürich, 8092 Zürich, Switzerland

[§]School of Physics and Astronomy, Cardiff University, The Parade, Cardiff CF243AA, United Kingdom

[∥]Institute of Inorganic Chemistry, Department of Chemistry and Applied Bioscience, ETH Zürich, 8093 Zürich, Switzerland

[⊥]Laboratory of Thin Films and Photovoltaics, Empa − Swiss Federal Laboratories for Materials Science and Technology, 8600 Dübendorf, Switzerland

[#]Cardiff University School of Biosciences, Museum Avenue, Cardiff CF10 3AX, United Kingdom

Supporting Information

ABSTRACT: Fully inorganic cesium lead halide perovskite nanocrystals (NCs) have shown to exhibit outstanding optical properties such as wide spectral tunability, high quantum yield, high oscillator strength as well as blinking-free single photon emission, and low spectral diffusion. Here, we report measurements of the coherent and incoherent exciton dynamics on the 100 fs to 10 ns time scale, determining dephasing and density decay rates in these NCs. The experiments are performed on $CsPbBr_2Cl$ NCs using transient resonant three-pulse four-wave mixing (FWM) in heterodyne detection at temperatures ranging from 5 to 50 K. We found a low-temperature exciton dephasing time of 24.5 ± 1.0 ps, inferred from the decay of the photon-echo amplitude at 5 K, corresponding to a homogeneous line width (fwhm) of 54 ± 5 μeV. Furthermore, oscillations in the photon-echo signal on a picosecond time scale are observed and attributed to coherent coupling of the exciton to a quantized phonon mode with 3.45 meV energy.

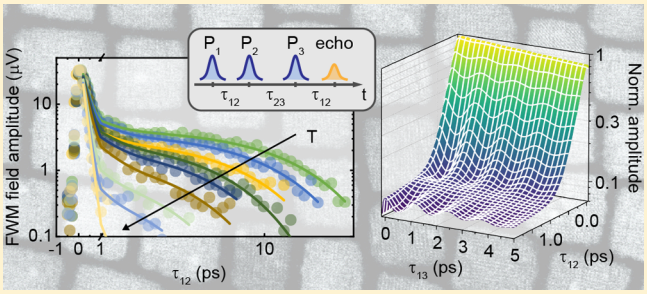

KEYWORDS: *Perovskite, nanocrystals, quantum dots, four wave mixing, photon echo, coherence, T_2, phonons, lead halide, heterodyne detection*

Recently, a new type of colloidal nanocrystals (NCs) has emerged for optoelectronic applications which combines simplicity in synthesis with great spectral flexibility and exceptional optical properties. Fully inorganic cesium lead halide perovskite NCs ($CsPbX_3$, where X = Cl, Br, I or mixture thereof)[1,2] have shown outstanding optical properties such as wide spectral tunability and high oscillator strength.[3] These NCs can be synthesized with precise compositional and size control and show room-temperature photoluminescence (PL) quantum yields (QY) of 60−90% (ref 1). Moreover, perovskite NCs have attracted much interest due to their large absorption coefficient and gain for optically pumped lasing devices.[4] At cryogenic temperatures, the PL decay is mostly radiative with lifetimes in the few hundred picosecond range, depending on size and composition of the NCs. This results from a "giant oscillator strength" in the intermediate confinement regime with an exciton Bohr radius of 5−7 nm for cesium lead bromide-chloride ($CsPbBr_2Cl$) NCs and a bright lowest triplet state manifold.[5] Furthermore, almost blinking-free single photon emission and marginal spectral diffusion have been reported for $CsPbX_3$ quantum dots at low temperature.[3,6] These remarkable features make perovskite-type lead halide NCs a prime candidate for the observation of strong light−matter interaction, e.g., showing coherent cooperative emission[7] or creating exciton-polaritons by embedding them in high-finesse optical cavities, as shown for CVD-grown fully inorganic lead halide perovskite nanowires[8,9] and nanoplatelets.[10] However, the time scale of such coherent coupling is limited by the exciton dephasing, which is still unknown for this material.

Transient four-wave-mixing (TFWM) spectroscopy is a powerful method allowing direct measurement of the loss of quantum coherence characterized by a dephasing time T_2. It has

Received: July 24, 2018
Revised: October 30, 2018
Published: November 8, 2018

DOI: 10.1021/acs.nanolett.8b03027
Nano Lett. XXXX, XXX, XXX−XXX

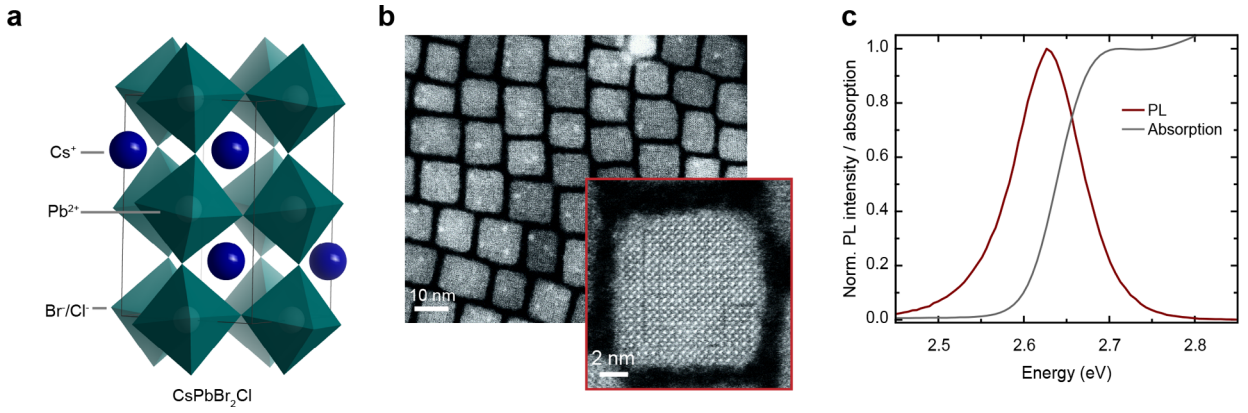

Figure 1. Crystal structure and optical properties of $CsPbBr_2Cl$ nanocrystals. (a) Fully inorganic perovskite cesium lead halide unit cell with typical quasi-cubic crystal structure with γ-orthorhombic distortion. (b) Transmission electron microscopy (TEM) image of $CsPbBr_2Cl$ nanocrystals (inset: single NC with high-resolution TEM). (c) Normalized ensemble PL and absorption spectra at 295 K.

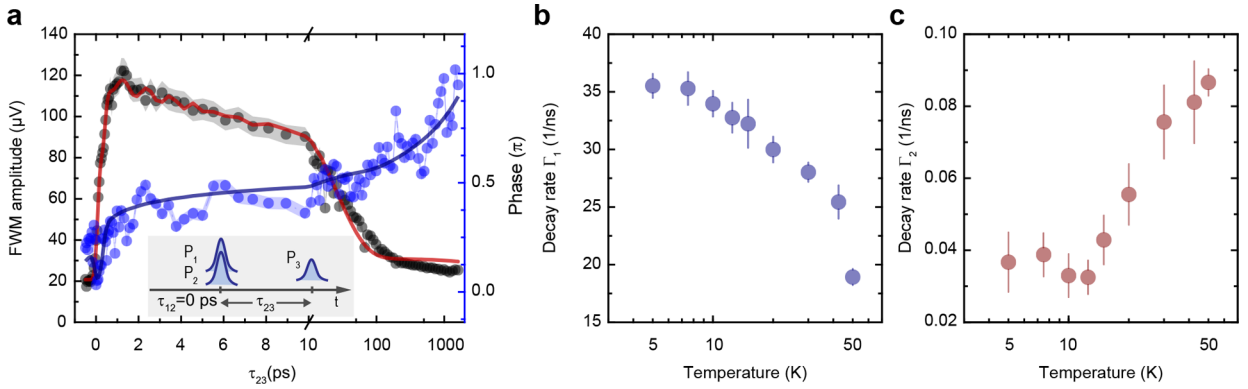

Figure 2. Temperature-dependent population density decay. (a) FWM field amplitude (black circles) and phase (blue circles) with their respective errors (shades) as a function of time delay τ_{23} between the first two pulses and the third pulse at 5 K. The solid lines represent fits to the data using the model discussed in the text. Inset: Sketch of the three-beam pulse sequence with $\tau_{12} = 0$ ps. (b) Decay rates Γ_1 and (c) Γ_2 of the two exponential decays extracted from the complex fit as a function of temperature.

been applied on various materials such as ruby crystals,[11] atoms,[12] molecules,[13,14] and semiconductor nanostructures.[15−17] In general, the dephasing of excitons in semiconductor materials is caused by elastic and inelastic scattering processes with phonons and charge carriers, and by radiative population decay.[18]

We studied the exciton dephasing and population dynamics using three-pulse degenerate TFWM spectroscopy on an ensemble of $CsPbBr_2Cl$ NCs. Previous measurements on colloidal CdSe-based NCs[19,20] and nanoplatelets[21] revealed a strong dependence of the T_2 time on the material and its shape and size. Also, FWM experiments on $MAPbI_3$ nanoplatelets reported a dephasing time of 800 fs and exciton quantum beating effects.[22] The investigated cubic $CsPbBr_2Cl$ NCs with edge lengths of 10 ± 1 nm were synthesized as discussed in the Supporting Information (SI) and possess the 3D-perovskite orthorhombic crystal structure (*Pnma* space group), shown in Figure 1a. Single quantum dot (QD) spectroscopy at cryogenic temperatures revealed that the emission of individual $CsPbBr_2Cl$ NCs exhibits a PL full-width at half-maximum (fwhm) below 1 meV, and a fine structure with an average energy splitting around 1 meV.[3,23] The exciton decay, measured at 5 K using nonresonant excitation, is mostly radiative with decay times of 180−250 ps. This is 1000 times faster than in CdSe/ZnS QDs[24] at cryogenic temperatures, and attributed to high oscillator strength due to larger exciton coherence volume, and the absence of a low-energy dark state.[5]

We performed TFWM experiments on films prepared by drop-casting a solution of NCs and polystyrene in toluene on *c*-cut quartz substrates (see SI). At room temperature, the PL emission (see Figure 1c) is centered at a photon energy of 2.63 eV and exhibits a Stokes shift of about 70 meV with respect to the ground-state exciton absorption resonance. At 5 K, the absorption peak red shifts to 2.61 eV, which is a known feature of lead-based semiconductor NCs such as PbS and PbSe,[25] as shown in the Supporting Information in Figure S5. The TFWM experiments have been performed by resonant excitation of the NCs at 2.58 eV with femtosecond pulses (120 fs intensity fwhm) from the second harmonic of a Ti:sapphire oscillator with 76 MHz repetition rate (for details of the experimental setup see Naeem et al., ref 21 and Scarpelli et al., ref 26). The first excitation pulse (P_1) with wavevector $\boldsymbol{k}_1$ induces a coherent polarization of the emitters in the inhomogeneous sample, which is then subject to dephasing. After a time delay τ_{12}, a second pulse (P_2) converts the polarization into a population density grating. The third pulse (P_3), which arrives on the sample after a time delay τ_{23}, is diffracted by the density grating, creating a FWM signal with a wavevector of $\boldsymbol{k}_S = \boldsymbol{k}_3 + \boldsymbol{k}_2 - \boldsymbol{k}_1$ (refs 20, 21). To investigate the exciton population dynamics, we set the time delay between the first and the second pulse to zero ($\tau_{12} = 0$ ps) and measure the FWM signal as a function of

DOI: 10.1021/acs.nanolett.8b03027
Nano Lett. XXXX, XXX, XXX−XXX

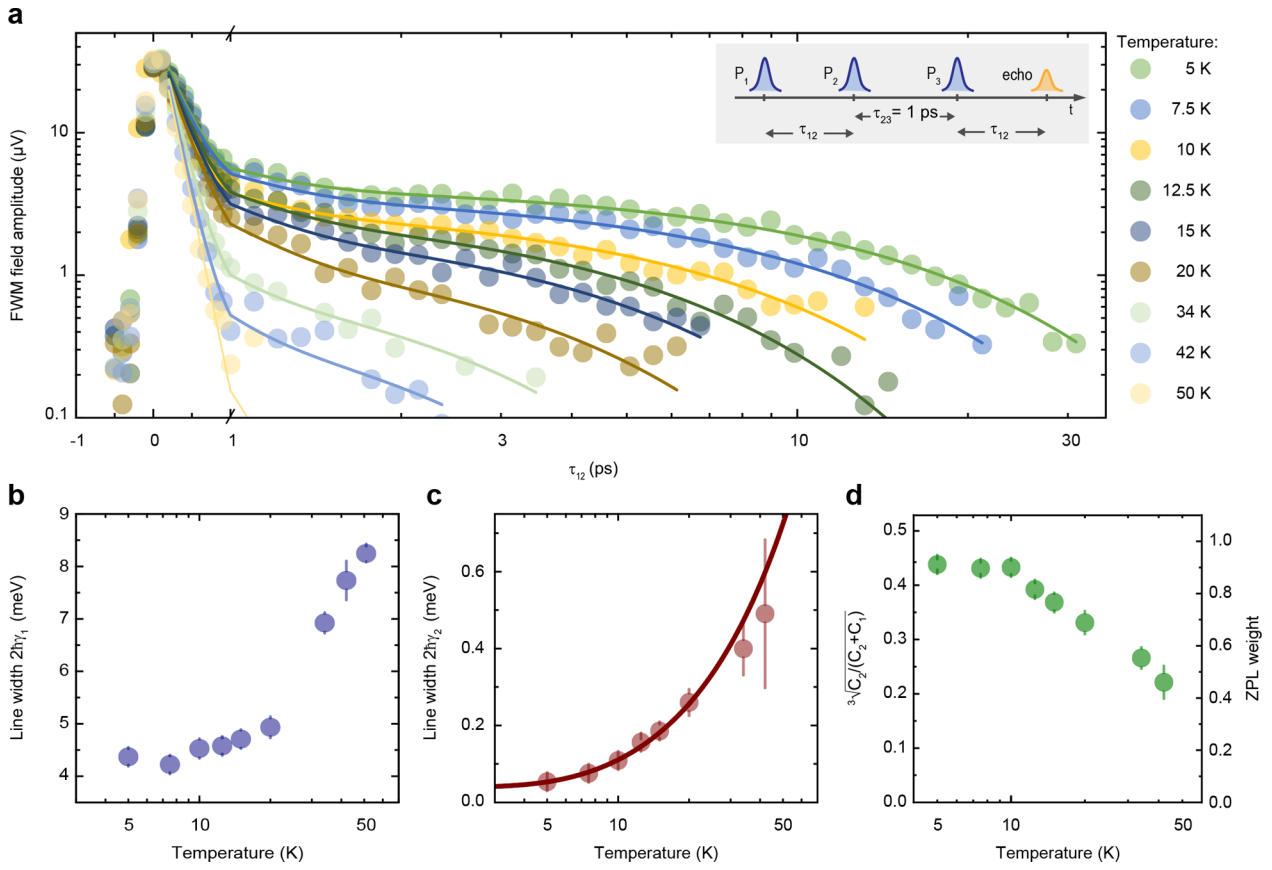

Figure 3. Temperature-dependent photon echo. (a) FWM field amplitude as a function of the time delay τ_{12} between the first and the second pulse in the temperatures range 5−50 K for fixed τ_{23} = 1 ps. Inset: Sketch of the three-beam pulse sequence and resulting photon echo. (b) Line width $2\hbar\gamma_1$ as a function of temperature. (c) Homogeneous line width $2\hbar\gamma_2$ as a function of temperature. The line is a weighted fit to the data. (d) Temperature dependence of the nominal ZPL weight (left vertical-axis) and the corrected ZPL weight (right vertical-axis).

the time delay τ_{23}. We use a spatial selection geometry to suppress the transmitted excitation pulses and then further discriminate the FWM signal from the exciting pulses using a heterodyne technique, in which the pulse train P_i is radio frequency shifted by Ω_i (i = 1, 2, 3), resulting in a frequency-shifted FWM field which is detected by its interference with a reference pulse.[21] In Figure 2a, the measured FWM field amplitude (black) and phase (blue) at 5 K with their respective fits are shown. We fit the amplitude and phase with a biexponential response function to quantify the population dynamics with decay rates $\Gamma_1 > \Gamma_2$, as explained in the SI. Superimposed onto the population decay, we observe in the initial dynamics damped oscillations with a period of about 1.2 ± 0.1 ps, which we interpret as coherent phonon interactions, as we will discuss in more detail further below.

At 5 K, the FWM field amplitude decays with two distinct time constants. The fast decay time τ_1 = 28.2 ± 0.8 ps with a relative amplitude of $\frac{A_1}{A_1+A_2}$ = 0.89 ± 0.07 (see Figure S4 in the Supporting Information) corresponds to a decay rate $\Gamma_1 = \frac{1}{\tau_1}$ = 35.5 ± 1.0 ns^{-1}, i.e. a line width of $\hbar\Gamma_1$ = 23.4 ± 2.0 μeV (Figure 2b). This rate is independent of excitation power (see Figure S3 in the Supporting Information), and we note that the decay rate is higher compared to nonresonantly excited PL.[5] A qualitatively similar difference between lifetimes observed in resonant FWM and nonresonant PL is observed in CdSe nanoplatelets[21] and CdSe/ZnS NCs[19]. It is attributed to the resonant excitation, selecting the states and nanocrystals in the ensemble with the highest oscillator strength, as observed in quantum wells with localized excitons.[27] Furthermore, in nonresonant PL, the dynamics can be influenced by the relaxation of the electron−hole pairs within the complex level structure by phonon-assisted processes. This relaxation can have time scales similar or substantially longer than the radiative lifetimes, thus affecting the measured PL decay times, as observed for CdSe nanoplatelets.[21] Because the lowest state in cesium lead halide NCs is bright,[5] relaxation to the dark state is not relevant at low temperature. With increasing temperature the decay rate Γ_1 is decreasing, which is interpreted to arise from occupation of the dark fine-structure state with the level structure proposed in ref 5.

The second decay component is 4 orders of magnitude slower, Γ_2 = 0.037 ± 0.009 ns^{-1} at 5 K, which is below the repetition rate in the experiment, and has a low weight of about 10% of the first one. In contrast to the first decay component, Γ_2 increases with temperature, as shown in Figure 2c. We assign the long decay component to the recombination time of trap or defect states present in a small fraction of the NCs, and their decay rate increases with temperature by thermal activation. Such decay on time scales of nanoseconds to milliseconds is often associated with trapping and detrapping of charge carriers or slow direct recombination in trap states, as observed with other colloidal NCs.[28] The relative amplitude of the components is temperature independent within error (see SI). The highest excitation density is estimated to excite up to 0.08

DOI: 10.1021/acs.nanolett.8b03027
Nano Lett. XXXX, XXX, XXX−XXX

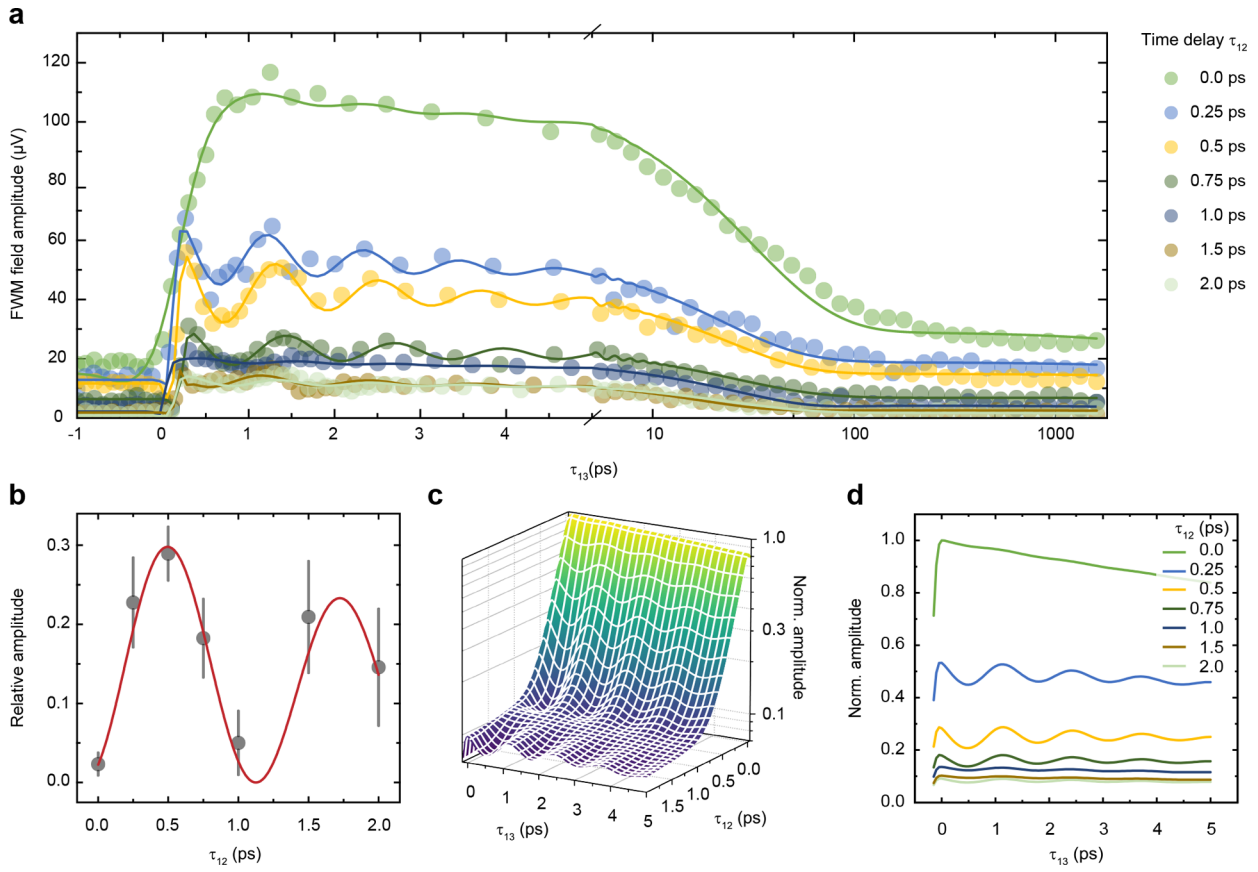

Figure 4. Coherent coupling to phonon modes. (a) Three-beam photon-echo field amplitude as a function of τ_{13} for various time delays τ_{12} at 5 K. Fits to the data (circles) are represented by solid lines. (b) Relative amplitude of the damped oscillation from the fits in (a) as a function of the time delay τ_{12}. The data are fitted with a damped sinusoidal function. (c) Calculated electric field of three-beam photon-echo signal for a two-level system coupled to a single harmonic mode as a function of τ_{12} and τ_{13} (linear scale). (d) Calculated three-beam photon-echo field amplitude for a two-level system coupled to a single harmonic mode for similar time delays as in (a).

excitons per excitation pulse per NC, ruling out significant multiexciton effects.

The dephasing time can be extracted from the decay of the photon echo, which we measured using three-pulse FWM spectroscopy in a heterodyne detection scheme (see SI). We scan the time delay τ_{12} between the first and the second pulse, while choosing a positive time delay τ_{23} = 1 ps to avoid instantaneous nonresonant nonlinearities.[21] The photon echo is then emitted at time τ_{12} after the third pulse P_3, as depicted in the inset of Figure 3a. The time-integrated FWM field amplitude as a function of delay time τ_{12} is shown in Figure 3a for various temperatures. The FWM amplitude shows a biexponential behavior up to 42 K. The initial fast decay of the amplitude proportional to $\exp(-2\gamma_1\tau_{12})$ in the time domain corresponds to a line width $2\hbar\gamma_1 = 4.37 \pm 0.16$ meV at 5 K. It is attributed to phonon-assisted transitions and a quantum beat of the fine-structure split states, which show a distribution of splittings in the meV energy range as they vary from NC to NC. Since the presence of an exciton in one of these states renormalizes all remaining exciton transitions into exciton−biexciton transitions, the density gratings of the states are adding up, constructively interfering at $\tau_{12} = 0$, and the beat with a wide distribution of frequencies results in a decay over the time scale of the inverse splitting. Assuming we excite the three bright states uniformly, a decay of the signal by a factor of 3 over the time scale of about a picosecond, given by the inverse energy splitting, is expected. Additionally, phonon-assisted transitions will contribute, as observed in other 3D confined systems.[19,20,29] However, the large extension of the excitons inside the individual NCs, which is the origin of the giant oscillator strength, is reducing their weight in the signal. This is confirmed in low-temperature single NC PL spectra, which do not show significant phonon-assisted emission, with an estimated zero phonon line (ZPL) weight of 0.93 (see SI). The line width of $2\hbar\gamma_1$ increases gradually as a function of temperature (Figure 3b). In general, the homogeneous line width of each fine-structure transition in the spectral domain is composed of a broad acoustic phonon band that corresponds to the fast initial dephasing, which is superimposed on a sharp Lorentzian-shaped ZPL, corresponding to the long exponential dephasing in the time domain.[29] From the second decay component of the photon echo, we can therefore deduce the ZPL width $2\hbar\gamma_2 = 54 \pm 5$ μeV, corresponding to a dephasing time $T_2 = 24.5 \pm 1.0$ ps at 5 K. In PL measurements of single NCs at 5 K, line widths of typically a few hundred μeV are found for $CsPbBr_2Cl$ NCs[3] (see SI). The value obtained by FWM is consistent with this, considering that fast spectral diffusion is typically affecting single NC PL.[30] The temperature dependence of the homogeneous line width is plotted in Figure 3c. The solid red line is a temperature-activated fit of the ZPL width using $2\hbar\gamma_2 = \hbar\gamma_0 + \frac{b}{e^{\Delta/k_BT} - 1}$, with the scattering energy $b = 0.23 \pm 0.09$ meV, and the zero-temperature extrapolated line width $\hbar\gamma_0 = 39.6 \pm 7.1$ μeV. The activation energy $\Delta = 1.23 \pm 0.35$ meV is consistent with the reported

DOI: 10.1021/acs.nanolett.8b03027
Nano Lett. XXXX, XXX, XXX−XXX

average fine-structure splitting from single NC spectroscopy measurements[5] (see SI), suggesting that phonon-assisted scattering into different fine-structure states is responsible for the dephasing. In Figure 3d the temperature dependence of the nominal ZPL weight $Z = \sqrt[3]{\frac{C_2}{C_1 + C_2}}$ is plotted, where C_1 and C_2 are the decay amplitudes of the fast and long decay component of the photon echo, respectively. The nominal ZPL weight is $Z = 0.44$ and remains constant up to 10 K and then starts to decrease with increasing temperature. As discussed above we attribute the initial decay of the photon echo mostly to an overdamped beat between the fine-structure states, so that the reported nominal ZPL weight is lower than the real ZPL weight of the individual bright transitions. For equal weights of three transitions in the fine-structure beat, the amplitude will decay by a factor of 3. Taking into account this decay results in a ZPL weight of 0.63 at 5 K. If we furthermore assume that the upper two fine-structure states are dephasing fast due to phonon-assisted transitions to the lowest state, there is an additional decay by a factor of 3. Taking all these corrections into account results in a ZPL weight of 0.91 at 5 K, as is shown in Figure 3d on the right vertical-axis. This weight is consistent with the ZPL weight 0.93 extracted from single NC PL (see SI). The overall temperature dependence of the corrected ZPL weight is similar to the one observed for epitaxial InGaAs QDs.[31] In CdSe colloidal quantum dots[19] instead, which have a much smaller exciton coherence volume, significantly stronger phonon-assisted transitions are present, with a ZPL weight of about 0.7 at 5 K, decaying to 0.4 at 20 K. However, the ZPL weight for temperatures below 12 K is found to be constant, in contrast to the two above-mentioned systems, which both show a continuous decrease of the ZPL weight with temperature. Notably, the phonon-assisted transitions in these other QD systems are dominated by coupling to a continuum of acoustic phonons with linear dispersion around zero momentum (Γ-point), resulting in a broad phonon-assisted band. The single QD PL of the perovskite NCs (see SI) instead shows no such broad band, but rather two well-defined phonon energies of about 3 and 6 meV. These discrete phonon energies would be expected to lead to an activated behavior of the ZPL weight reduction, consistent with the observed constant ZPL weight below 12 K.

To further investigate the initial oscillations in the density dynamics in Figure 2a, we took data for different delays $\tau_{12} \geq 0$. The resulting FWM field amplitude as a function of τ_{13} is shown in Figure 4a. The amplitude of the oscillations changes while the oscillation period remains stable at $\tau_0 = 1.20 \pm 0.05$ ps. The relative amplitudes B of the damped oscillations are shown in Figure 4b as a function of time delay τ_{12}, exhibiting an oscillating behavior. The red curve displays a fit with a damped squared-sine function. From this, an oscillation period of 1.22 ± 0.02 ps is obtained, which concurs with the period of the initial oscillations in the density decay. We therefore attribute these oscillations to coherent exciton−phonon coupling, resulting from the modulated polarization as a function of the harmonic nuclei displacement, as previously reported for CdSe NCs,[32,33] PbS NCs[34] and $CsPbCl_3$ NCs[35] in a CsCl matrix. The resulting vibrational energy of 3.45 ± 0.14 meV is in good agreement with the measured phonon energies of phonon-assisted transitions in single NC PL measurements (see SI), which have been attributed to optical phonon modes in bulk $CsPbCl_3$[36] and for individual $CsPbBr_3$ NCs.[23] The definitive attribution of the phonon replica to a longitudinal optical (LO) or to a transverse optical (TO) phonon mode remains difficult since the observed and calculated phonon frequencies in bulk for TO- and LO-phonons are very close to each other.[37,38] The oscillation damping could be due to (i) decay of the phonon mode into acoustic phonons[33] or vibronic modes of the ligands/polystyrene matrix and (ii) inhomogeneous broadening of the phonon mode in the QD ensemble, as observed in $FAPbBr_3$ NCs.[39] The damping time $\tau_{damp} = 2.3 \pm 0.7$ ps would correspond to an energy dispersion of 0.6 ± 0.2 meV, close to the value of 0.5 meV measured for the phonon energy inhomogeneous broadening in $FAPbBr_3$ NCs.[39] The three-pulse photon-echo signal $S(\tau_{12}, \tau_{13})$ in the direction $\boldsymbol{k}_S = -\boldsymbol{k}_1 + \boldsymbol{k}_2 + \boldsymbol{k}_3$ of an inhomogeneously broadened two-level system coupled to a single harmonic mode of angular frequency ω can be calculated as[33,40]

$$S(\tau_{12}, \tau_{13}) \approx \exp[-4\Delta^2(n(\omega) + 1)\cdot(1 - \cos(\omega\tau_{12}))(1 - \cos(\omega\tau_{13}))]\cdot\exp\left(-\frac{4\tau_{12}}{T_2}\right)\cdot\exp\left(-\frac{2\tau_{13}}{T_1}\right)\cdot\Phi(\tau_{12}, \tau_{13}) \quad (1)$$

Here, ω is the mode frequency and $n(\omega) = 1/\left[\exp\left(\frac{\hbar\omega}{k_B T}\right) - 1\right]$ is the Bose occupation factor. The function $\Phi(\tau_{12}, \tau_{13}) = 1 + \cos(\Delta^2[\sin(\omega\tau_{12}) - \sin(\omega\tau_{13}) + \sin(\omega\tau_{13} - \omega\tau_{12})])$ arises from the superposition of different Liouville space pathways.[41] Δ represents the coupling factor between excitonic state and phonon mode and can be expressed by the Huang−Rhys parameter. For further details, we refer to the work of Mittlemann and Schoenlein et al.[32,33] In Figure 4c, we show the modeled electric fields of the three-pulse photon echo with $E(\tau_{12}, \tau_{23}) \approx \sqrt{S(\tau_{12}, \tau_{23})}$ according to eq 1. The model uses a Huang−Rhys parameter of $\frac{1}{2}\Delta^2 = 0.038$, a phonon mode at 3.45 meV (as measured in single NC PL measurements, see SI), and the above measured decay rates Γ_1 and $\gamma_{1,2}$ with their corresponding amplitudes. We have included an oscillation damping ($\tau_{damp} = 2.5$ ps) and a finite pulse duration by multiplying $S(\tau_{12}, \tau_{13})$ with $\frac{1}{4}\left(1 + \mathrm{erf}\left(\frac{\tau_{12}}{\tau_0}\right)\right)\left(1 + \mathrm{erf}\left(\frac{\tau_{13}}{\tau_0}\right)\right)$, where $\tau_0 = 72$ fs describes the amplitude fwhm using the intensity fwhm $2\sqrt{\ln 2}\,\tau_0 = 120$ fs of the excitation pulses. The complete formula is provided in the SI. For better comparison with experiment, the calculated photon-echo signals for the experimental time delays are plotted in Figure 4d and Figure S6 in the Supporting Information, from which good agreement with measurements can be inferred.

In conclusion, we have investigated the coherence and density dynamics in fully inorganic $CsPbBr_2Cl$ NCs at cryogenic temperatures. Using three-beam FWM, we obtain a dephasing time and a density decay time of several tens of picoseconds at 5 K. Furthermore, we find excitation of coherent phonons of 3.45 meV energy with a Huang−Rhys parameter of 0.038. The observed long dephasing time close to the lifetime limit is promising for applications in microcavity devices based on strong light−matter interaction.

DOI: 10.1021/acs.nanolett.8b03027
Nano Lett. XXXX, XXX, XXX−XXX

■ ASSOCIATED CONTENT

Supporting Information

The Supporting Information is available free of charge on the ACS Publications website at DOI: 10.1021/acs.nanolett.8b03027.

Synthesis and material characterization details, optical spectroscopy and heterodyne detected four-wave mixing methods, data analysis procedures and algorithms (PDF)

■ AUTHOR INFORMATION

Corresponding Authors

*mvkovalenko@ethz.ch (M.V.K.).
*langbeinww@cardiff.ac.uk (W.L.).
*rfm@zurich.ibm.com (R.F.M.).

ORCID

Thilo Stöferle: 0000-0003-0612-7195
Maksym V. Kovalenko: 0000-0002-6396-8938
Rainer F. Mahrt: 0000-0002-9772-1490

Notes

The authors declare no competing financial interest.

■ ACKNOWLEDGMENTS

The authors acknowledge helpful discussions with D. J. Norris. M.A.B., G.R., M.V.K., T.S., and R.F.M. acknowledge the European Union's Horizon-2020 program through the Marie-Sklodowska Curie ITN network "PHONSI" (H2020-MSCA-ITN-642656) and the Swiss State Secretariat for Education Research and Innovation (SERI). L.S., F.M., and W.L. acknowledge partial funding from EPSRC by Grants EP/M020479/1 and EP/M012727/1.

■ REFERENCES

(1) Protesescu, L.; Yakunin, S.; Bodnarchuk, M. I.; Krieg, F.; Caputo, R.; Hendon, C. H.; Yang, R. X.; Walsh, A.; Kovalenko, M. V. *Nano Lett.* **2015**, *15*, 3692−3696.

(2) Nedelcu, G.; Protesescu, L.; Yakunin, S.; Bodnarchuk, M. I.; Grotevent, M. J.; Kovalenko, M. V. *Nano Lett.* **2015**, *15*, 5635−5640.

(3) Rainò, G.; Nedelcu, G.; Protesescu, L.; Bodnarchuk, M. I.; Kovalenko, M. V.; Mahrt, R. F.; Stöferle, T. *ACS Nano* **2016**, *10*, 2485−2490.

(4) Yakunin, S.; Protesescu, L.; Krieg, F.; Bodnarchuk, M. I.; Nedelcu, G.; Humer, M.; De Luca, G.; Fiebig, M.; Heiss, W.; Kovalenko, M. V. *Nat. Commun.* **2015**, *6*, 8056.

(5) Becker, M. A.; Vaxenburg, R.; Nedelcu, G.; Sercel, P. C.; Shabaev, A.; Mehl, M. J.; Michopoulos, J. G.; Lambrakos, S. G.; Bernstein, N.; Lyons, J. L.; Stöferle, T.; Mahrt, R. F.; Kovalenko, M. V.; Norris, D. J.; Rainò, G.; Efros, A. L. *Nature* **2018**, *553*, 189−193.

(6) Yin, C.; Chen, L.; Song, N.; Lv, Y.; Hu, F.; Sun, C.; Yu, W. W.; Zhang, C.; Wang, X.; Zhang, Y.; Xiao, M. *Phys. Rev. Lett.* **2017**, *119*, No. 026401.

(7) Rainò, G.; Becker, M. A.; Bodnarchuk, M. I.; Mahrt, R. F.; Kovalenko, M. V.; Stöferle, T. *Nature*. DOI: 10.1038/s41586-018-0683-0, Published Online Nov 7, 2018. https://www.nature.com/articles/s41586-018-0683-0.

(8) Evans, T. J. S.; Schlaus, A.; Fu, Y.; Zhong, X.; Atallah, T. L.; Spencer, M. S.; Brus, L. E.; Jin, S.; Zhu, X.-Y. *Adv. Opt. Mater.* **2018**, *6*, 1700982.

(9) Du, W.; Zhang, S.; Shi, J.; Chen, J.; Wu, Z.; Mi, Y.; Liu, Z.; Li, Y.; Sui, X.; Wang, R.; Qiu, X.; Wu, T.; Xiao, Y.; Zhang, Q.; Liu, X. *ACS Photonics* **2018**, *5*, 2051−2059.

(10) Su, R.; Diederichs, C.; Wang, J.; Liew, T. C. H.; Zhao, J.; Liu, S.; Xu, W.; Chen, Z.; Xiong, Q. *Nano Lett.* **2017**, *17*, 3982−3988.

(11) Kurnit, N. A.; Abella, I. D.; Hartmann, S. R. *Phys. Rev. Lett.* **1964**, *13* (19), 567−568.

(12) Mossberg, T.; Flusberg, A.; Kachru, R.; Hartmann, S. R. *Phys. Rev. Lett.* **1979**, *42*, 1665−1670.

(13) Becker, P. C.; Fragnito, H. L.; Bigot, J. Y.; Brito Crus, C. H.; Fork, R. L.; Shank, C. V. *Phys. Rev. Lett.* **1989**, *63*, 505−507.

(14) Nibbering, E. T. J.; Wiersma, D. A.; Duppen, K. *Phys. Rev. Lett.* **1991**, *66*, 2464−2467.

(15) Leo, K.; Wegener, M.; Shah, J.; Chemla, D. S.; Göbel, E. O.; Damen, T. C.; Schmitt-Rink, S.; Schäfer, W. *Phys. Rev. Lett.* **1990**, *65*, 1340−1343.

(16) Kim, D.-S.; Shah, J.; Damen, T. C.; Schäfer, W.; Jahnke, F.; Schmitt-Rink, S.; Köhler, K. *Phys. Rev. Lett.* **1992**, *69*, 2725−2728.

(17) Schultheis, L.; Kuhl, J.; Honold, A.; Tu, C. W. *Phys. Rev. Lett.* **1986**, *57*, 1635−1638.

(18) Shah, J. *Ultrafast Spectroscopy of Semiconductors and Semiconductor Nanostructures*; Springer: Berlin, Heidelberg, 1996.

(19) Masia, F.; Accanto, N.; Langbein, W.; Borri, P. *Phys. Rev. Lett.* **2012**, *108*, No. 087401.

(20) Masia, F.; Langbein, W.; Moreels, I.; Hens, Z.; Borri, P. *Phys. Rev. B: Condens. Matter Mater. Phys.* **2011**, *83*, No. 201309(R).

(21) Naeem, A.; Masia, F.; Christodoulou, S.; Moreels, I.; Borri, P.; Langbein, W. *Phys. Rev. B: Condens. Matter Mater. Phys.* **2015**, *91*, No. 121302(R).

(22) Bohn, B. J.; Simon, T.; Gramlich, M.; Richter, A. F.; Polavarapu, L.; Urban, A. S.; Feldmann, J. *ACS Photonics* **2018**, *5*, 648−654.

(23) Fu, M.; Tamarat, P.; Huang, H.; Even, J.; Rogach, A. L.; Lounis, B. *Nano Lett.* **2017**, *17*, 2895−2901.

(24) Crooker, S. A.; Barrick, T.; Hollingsworth, J. A.; Klimov, V. I. *Appl. Phys. Lett.* **2003**, *82*, 2793−2795.

(25) Olkhovets, A.; Hsu, R.-C.; Lipovskii, A.; Wise, F. W. *Phys. Rev. Lett.* **1998**, *81*, 3539−3542.

(26) Scarpelli, L.; Masia, F.; Alexeev, E. M.; Withers, F.; Tartakovskii, A. I.; Novoselov, K. S.; Langbein, W. *Phys. Rev. B: Condens. Matter Mater. Phys.* **2017**, *96*, No. 045407.

(27) Langbein, W.; Patton, B. *Phys. Rev. Lett.* **2005**, *95*, No. 017403.

(28) Rabouw, F. T.; Kamp, M.; van Dijk-Moes, R. J. A.; Gamelin, D. R.; Koenderink, A. F.; Meijerink, A.; Vanmaekelbergh, D. *Nano Lett.* **2015**, *15*, 7718−7725.

(29) Borri, P.; Langbein, W.; Schneider, W.; Woggon, U.; Sellin, R. L.; Ouyang, D.; Bimberg, D. *Phys. Rev. Lett.* **2001**, *87*, No. 157401.

(30) Biadala, L.; Frederich, H.; Coolen, L.; Buil, S.; Quélin, X.; Javaux, C.; Nasilowski, M.; Dubertret, B.; Hermier, J.-P. *Phys. Rev. B: Condens. Matter Mater. Phys.* **2015**, *91*, No. 085416.

(31) Borri, P.; Langbein, W.; Woggon, U.; Stavarache, V.; Reuter, D.; Wieck, A. D. *Phys. Rev. B: Condens. Matter Mater. Phys.* **2005**, *71*, No. 115328.

(32) Schoenlein, R. W.; Mittleman, D. M.; Shiang, J. J.; Alivisatos, A. P.; Shank, C. V. *Phys. Rev. Lett.* **1993**, *70*, 1014−1017.

(33) Mittleman, D. M.; Schoenlein, R. W.; Shiang, J. J.; Colvin, V. L.; Alivisatos, A. P.; Shank, C. V. *Phys. Rev. B: Condens. Matter Mater. Phys.* **1994**, *49*, 14435−14447.

(34) Krauss, T. D.; Wise, F. W. *Phys. Rev. Lett.* **1997**, *79*, 5102−5105.

(35) Němec, P.; Nitsch, K.; Nikl, M.; Malý, P. *Phys. Status Solidi C* **2004**, *1*, 2670−2673.

(36) Calistru, D. M.; Mihut, L.; Lefrant, S.; Baltog, I. *J. Appl. Phys.* **1997**, *82*, 5391−5395.

(37) Sendner, M.; Nayak, P. K.; Egger, D. A.; Beck, S.; Müller, C.; Epding, B.; Kowalsky, W.; Kronik, L.; Snaith, H. J.; Pucci, A.; Lovrinčić, R. *Mater. Horiz.* **2016**, *3*, 613−620.

(38) Pérez-Osorio, M. A.; Milot, R. L.; Filip, M. R.; Patel, J. B.; Herz, L. M.; Johnston, M. B.; Giustino, F. *J. Phys. Chem. C* **2015**, *119*, 25703−25718.

(39) Pfingsten, O.; Klein, J.; Protesescu, L.; Bodnarchuk, M. I.; Kovalenko, M. V.; Bacher, G. *Nano Lett.* **2018**, *18* (7), 4440−4446.

(40) Mukamel, S. *Principles of Nonlinear Optics and Spectroscopy*; Oxford University Press: New York, 1995.

(41) Yan, Y. J.; Mukamel, S. *J. Chem. Phys.* **1991**, *94*, 179−190.

DOI: 10.1021/acs.nanolett.8b03027
Nano Lett. XXXX, XXX, XXX−XXX